Lignin Nanoparticle Nucleation and Growth on Cellulose and Chitin Nanofibers

Eva Pasquier, Bruno Mattos, Naceur Belgacem, Julien Bras, Orlando Rojas

Pasquier, Eva; Mattos, Bruno D.; Belgacem, Naceur; Bras, Julien; Rojas, Orlando J.

Lignin Nanoparticle Nucleation and Growth on Cellulose and Chitin Nanofibers

Published in:
Biomacromolecules

DOI:
10.1021/acs.biomac.0c01596

Published: 08/02/2021

Document Version
Peer-reviewed accepted author manuscript, also known as Final accepted manuscript or Post-print

Please cite the original version:
Pasquier, E., Mattos, B. D., Belgacem, N., Bras, J., & Rojas, O. J. (2021). Lignin Nanoparticle Nucleation and Growth on Cellulose and Chitin Nanofibers. *Biomacromolecules*, *22*(2), 880-889. Article 0c01596. https://doi.org/10.1021/acs.biomac.0c01596

Lignin nanoparticle nucleation and growth on cellulose and chitin nanofibers

Eva Pasquier[a,b], Bruno D. Mattos[b], Naceur Belgacem[a,c], Julien Bras[a,c,±], Orlando J. Rojas[b,d]

[a] *Université Grenoble Alpes, CNRS, Grenoble INP (*Institute of Engineering*), LGP2, F-38000 Grenoble, France*

[b] *Department of Bioproducts and Biosystems, School of Chemical Engineering, Aalto University, P.O. Box 16300, Aalto, Espoo FIN-00076, Finland*

[c] *Institut Universitaire de France (IUF), 75000 Paris, France*

[d] *Bioproducts Institute, Departments of Chemical and Biological Engineering, Chemistry and Wood Science, University of British Columbia, 2360 East Mall, Vancouver, BC V6T 1Z3, Canada*

KEYWORDS: lignin, cellulose nanofibers, chitin nanofibers, biocolloids, sustainable films, packaging, bioeconomy.

ABSTRACT

Cellulose (CNF) and chitin (ChNF) nanofibers are known to form materials that are both tough and strong. In this study, we hypothesize that the inertness of networks associated to CNF and ChNF makes them ideal templates for heterogenous reaction engineering and to install functionalities by *in-situ* formation of nanoarchitectures. We expand nanoparticles templating on polysaccharide colloids by introducing a new and facile process that leads to the growth of organic nanoparticles on CNF and ChNF suspended in water. The process based on solvent shifting supported on solid interfaces is demonstrated by direct observation and exploits the photocatalytic effect of lignin nanostructures. Importantly, the dynamics of nanoparticles nucleation and growth is correlated to the surface chemistry of the templates. Electrostatic repulsion between the deprotonated lignin molecules and the slightly negative CNF support led to limited adsorption and, therefore, was effective in producing free (non-bound) lignin nanoparticles (28±7 nm) by precipitation. In contrast, the stronger interfacial interactions between the positively charged ChNF and lignin molecules led to instantaneous and extensive lignin adsorption, followed by nucleation and growth into relatively larger nanosphere (46±17 nm). The latter were homogeneously distributed and strongly coupled to the ChNF support. Overall, we introduce lignin nanoparticle nucleation and growth on renewable nanofibers as an effective route toward *in situ* synthesis of highly functional fibrils and derived cohesive films that offer great potential in packaging and other areas.

INTRODUCTION

Materials assembled from polysaccharide nanofibrillar networks are known for their remarkable mechanical performance. Highly cohesive structures arise from the interconnectivity and entanglement of high-aspect ratio nanofibers, which leads to a high density of physical crosslinks.[1,2] Fibrillar biocolloids, such as cellulose (CNF) and chitin (ChNF) nanofibers, are amongst the most suitable building blocks for the development of materials. This is due to their high strength, flexibility and morphology that yield tight, interconnected nanonetworks upon drying from aqueous media.[3–5] Unlike covalent bonding, supramolecularly-driven colloidal interactions can readily reform after bond breaking under mechanical stress, leading to a cascade of short-range bond breaking/reforming events that yield materials that are both tough and strong.[6] Moreover, the biological and chemical inertness of CNF and ChNF make them ideal supports for selective incorporation of functionalities, such as hydrophobicity, flame retardancy or conductivity, among others.[7–9] Compositing with nanoparticles (so far mostly inorganic), represents a low-energy route to introduce functionalities in CNF or ChNF matrices,[10,11] avoiding the need for the otherwise typical non-sustainable, expensive and time-consuming protocols used for chemical modification.[12]

Here we demonstrate the introduction of functional nanoparticles within nanofibrillar matrices by simply mixing and *in-situ* nucleation. The latter provides better control over particle-fiber interactions and the associated morphologies of the resulting networks. Nucleation of metallic nanoparticles on biobased nanofibers have been shown to produce high formation yields and, simultaneously, leads to a good dispersion of narrow sized nanoparticles across the network.[13,14] Nucleation and growth take place from the adsorption of the metallic precursor on the nanofibrils surface followed by the reduction of the precursor with the addition of an external reagent. Interactions between given precursors and supporting nanofibers, their nature and strength, have been shown to be key factors to enable efficient functionalization. For

instance, Olsson et al. successfully synthesized fully anchored cobalt ferrite ($CoFe_2O_4$) nanoparticles using nanocellulose aerogel templates. In their work, the initial Fe/Co metal cations adsorbed on the nanocellulose surface interacted strongly with the formed complexes in the liquid phase, leading to the absence of free nanoparticles in the system.[15] Padalkar et al. used a cationic surfactant to monitor the interactions between cellulose nanocrystals and metallic ions (Ag, Au, Cu, Pt) for the formation of supported nanoparticles.[16] Using similar protocols, Errokh et al. used modified CNFs as templates for the synthesis of silver nanoparticles, aiming at anti-microbial composites with limited silver release.[17] Although related formation mechanisms are not fully understood, it is known that interfacial interactions play a determining role for the nucleation and *in-situ* growth of metallic nanoparticles on biobased nanofibers. Much less is known in relation to the formation of organic nanoparticles on biobased templates, which is a subject that deserves attention, especially given the prospective uses of such systems.

Here we investigated the use of biobased nanofibers – CNF and ChNF – as nucleating solid supports for the formation of organic lignin nanoparticles (LPs). The latter results in a fully bio-based material, which can potentially address concerns related to the generation of microplastics from synthetic polymers used in packaging materials. The polyphenolic nature of lignin leads to interesting photocatalytic effects, such as UV shielding and antioxidant activity, which are especially relevant for food packaging considering that light is very detrimental for food.[18] Lignin colloids have also been explored in sunscreens applications[19] and recent developments indicate a great promise for nanocellulose in cosmetics. Thus, lignin can bring great benefits if incorporated in fibrillar matrices, especially in the form of nanoparticles which could be exploited to impart improved mechanical performance.[20,21]

In this study, we propose a new method for creating tailorable particle-fibers nanonetworks with better control over their final morphology by exploring interfacial interactions during the

heterogenous nucleation and growth of lignin nanoparticles. Our method is inspired by the solvent shifting method, which is scalable, low cost and leads to round-shaped particles.[22,23] We use chitin (positively charged) and cellulose (slightly negatively charged) nanofibers as templates to investigate the effects of such different nucleation sites for the *in-situ* formation of lignin constructs (**Figure 1**). We discuss adsorption and interfacial phenomena in relation to the biocolloidal components to better understand the interactions involved during the formation process. Lastly, films were synthesized from our hybrid colloidal suspensions, aiming to combine the ability of the nanofibers to create strong materials with the lignin photocatalytic properties, offering a viable platform for application in films for food packaging.

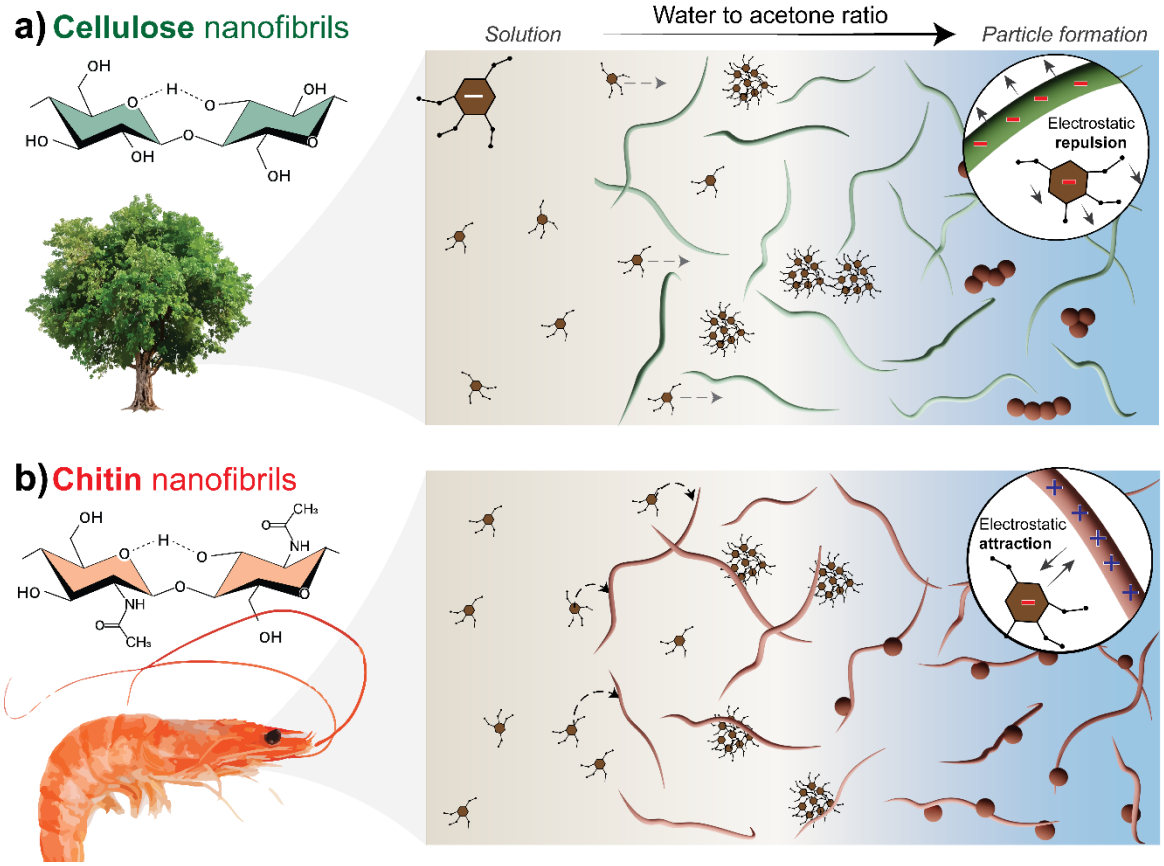

Figure 1. Schematic illustration of the solvent exchange process that leads to the nucleation and growth of lignin nanoparticles in the presence of **a)** cellulose and **b)** chitin nanofibers, both of which acted as templating supports. From an increased water-to-acetone ratio, lignin nanoparticles (LPs) were formed with a morphology that is controlled by the surface chemistry of the nanofibers. As such, LPs are formed loosely in suspension with non-interacting cellulosic templates. Conversely, strongly anchored LPs were formed on the surface of the chitin nanofibers, *via* electrostatic effect.

EXPERIMENTAL SECTION

Materials. Technical Kraft lignin (Indulin AT) from softwood was obtained from MeadWestvaco (USA). Cellulose nanofibers (CNF) were provided by the Centre Technique du Papier (CTP, Grenoble, France). Cellulose was sourced from bleached birch pulp refined and enzymatically pre-treated before homogenization (3 passes at 1500 bars) with an Ariete homogenizer from GEA (Italy). Chitin flakes of shrimp shells, $K_2S_2O_8$, and ABTS were purchased from Sigma Aldrich and acetone >99.5%, KOH, NaOH, HCl from Roth, all chemicals were used as received.

Chitin nanofibers production. Chitin nanofibers (ChNF) were produced from chitin flakes of shrimp shells; the purification of the fibers followed the procedure of Ifuku et al.[24] First, residual proteins were removed with KOH (5 wt%, 6 h, 100 °C). After washing to neutral pH, the fibers were soaked in HCl (5 %, 48 h, 25 °C) to remove any minerals. Then, another deproteinization step was conducted with KOH (5 wt%, 48 h, 25 °C) followed by bleaching with sodium chlorite (2 h at 80 °C). Finally, the fibers were defibrillated with a grinder (Masuko) to obtain chitin nanofibers (ChNF).

***In-situ* preparation of lignin particles**. The in-situ preparation of lignin particles was adapted from the classic solvent shifting method[25] but in the presence of nanofibers in the anti-solvent medium (water). For this purpose, 50 mg of lignin were dissolved in acetone:water (9:1) at 2 g/L. After mixing for 1 h, the solution was filtrated and the filtrate was dropped into 100 mL of a suspension of dispersed cellulose (CNF) or chitin (ChNF) nanofibers at 0.5 %, aiming at a final lignin content of 9%. As a reference, the same experiment was conducted in the absence of nanofibers. In addition, suspensions with 15% and 23% of lignin were also prepared with chitin nanofibers. The proportion of each component was always calculated on a dry mass basis.

Characterization of the suspensions. *Morphology.* The colloidal suspensions were imaged with transmission electron microscopy (TEM) using a JEOL JEM 2100-Plus microscope operating at 200 kV. Samples were dropped on copper grids and uranyl acetate was used as negative staining. At least 10 images were obtained by samples and the most representative is used for the discussions. Lignin particle size was measured from TEM images using Image J software with at least 100 measurements using at least three different images.

Surface charge measurement. The zeta-potential of the nanofibers before and after lignin particles preparation was measured with a Zetasizer Nano ZS (Malvern Panalytical) with a folded capillary cell. The concentration of the suspensions was 0.1 wt.% and their conductivity was adjusted to 0.65 mS/cm. The average of three measurements was used in the discussion.

Hydrodynamic size measurement. The size of the lignin particles was evaluated by dynamic light scattering (DLS) in a VASCO device (Cordouan Technologies), using the Cumulant method. The suspension was diluted around 0.05 wt.% before measurements.

Lignin quantification by UV spectroscopy. To understand the interactions between lignin and the nanofibers, a separation by centrifugation was carried out and lignin was quantified in the sediment. After centrifugation at 10 000 rpm for 5 min, the supernatant containing the LP and the sediment containing the nanofibers were separated and the sediment was washed 2 times with water, to remove residual LP. Lee et al.[26] showed that it was possible to quantify the amount of dissolved lignin with UV-Vis spectroscopy after dissolution in NaOH. Following their method, dissolution of the lignin present in the sediment with NaOH 0.035 M was carried out; for this purpose, NaOH was added to the sediment and dissolved lignin was collected after centrifugation (10 000 rpm, 5 min). The dissolution was repeated two more times to extract the lignin. After bringing the supernatants together, the solutions were analyzed with UV spectroscopy (UV-1800, Shimadzu). Dilution was done when necessary. To quantify the

lignin, a calibration curve with known amount of lignin dissolved in NaOH 0.035 M was performed beforehand.

Lignin interactions with the nanofibers. Paper chromatography was used to study the interactions between dissolved lignin and the nanofibers. First, the stationary phase was prepared; for this purpose, chromatography paper was coated with 0.5 % nanofibers suspension using a bar coater (K Control Coater, RK Print Coat Instruments Ltd.). A spirally-wound bar with 0.25 mm wire diameter was used, leading to a wet coating thickness of 150 µm. The coatings were dried in an oven at 105°C. The mobile phase was composed of an acetone:water mixture (4:6 v:v); the ratio was optimized to obtain a suitable result. Lignin was dissolved in acetone:water (9:1 v:v) and filtrated similarly to the lignin solution used for lignin particle preparation. A drop of 5 µL solution was deposited on the coated paper and the paper was placed in a beaker containing the mobile phase. Image analysis was performed with Python, after cropping the image; the full images were analyzed averaging the blue pixel values of each line. The image length was normalized for comparison purposes.

Films preparation. Films were prepared for a grammage of 47 g/m^2. Therefore, a given suspension volume was cast on PTFE Petri dish and degassed, to avoid bubbles in the suspension. The suspensions were dried at 50 % relative humidity (RH) and 25 °C. The films were acclimated at 50 % RH and 25°C before analysis.

Characterization of the films. All films were stored at least 24h in 50% RH and 25°C before characterization. *Mechanical strength.* Tensile tests were conducted with a dynamic mechanical analyzer device (DMA) (TA Instruments RSA 3), with a rate of 0.1 mm/s and a gap between the clamping jaws of 15 mm. Strips of 0.5 cm width were cut in the films, and their thickness and exact width were measured before analyses.

Scanning Electron Microscopy (SEM). The film morphology was studied with a SEM (FEI Quanta 200), films were broken in liquid nitrogen and the cross-section was imaged. Metallization with carbon was done before imaging.

Atomic Force Microscopy (AFM). The film's top surface was imaged with a Dimension Icon AFM (Bruker) operated in tapping mode. Samples of the films were attached to a support with double-sided tape. At least 3 images were obtained from the samples and the most representative ones were used for discussion.

Transparency. Transmittance of the films was measured with a UV-Vis spectrophotometer (Shimadzu) from 200 nm to 800 nm.

Wettability. Water contact angles were measured with an OCA20 device, equipped with a CCD camera, using a drop volume of 5 µL. Measurement were repeated at least 3 times and the angle was measured after 2 min of contact, using the SCA20 software.

Antioxidant activity. The radical scavenging capacity of the films was determined using 2,2'-azino-bis(3-ethylbenzothiazoline-6-sulphonic acid) (ABTS). First, a stock solution of radical was prepared mixing 18 mg of ABTS with and 3.3 mg of potassium persulfate as an oxidant to form the radical $ABTS^{+\bullet}$ in 5 mL of water.[27] After overnight reaction, the solution was diluted in order to have 20 mL solution with an absorbance of 0.8 at 734 nm. This solution was divided equally in two vials: the first one was the reference and 3 mg of films were added to the second one. The decrease in absorbance at 734 nm was measured as function of time as the film reacted with the radical. The radical scavenging activity was calculated following Equation 2:

$$RSA\ (\%) = \ 100 - \frac{A_{ref} - A_{sample}}{A_{ref}} \times 100$$

With A_{ref} the absorbance of the reference solution, and A_{sample} the absorbance of the sample at a given time. Tannic acid was used as a model molecule to compare the samples. For this purpose, the same experiment was realized but instead of a film, different quantities of tannic acid were added to the radical solution, and after calculation of the RSA, a calibration curve of

the RSA as a function of the mass of tannic acid was plotted. The Tannic Acid Equivalent (TAE) was calculated by dividing the equivalent mass of tannic acid reaching the same RSA than the sample by the mass of the film. All the comparisons were made after one hour of reaction with the radical solution.

Particles release study. Release of lignin and lignin particles from the films was studied in the same conditions than the antioxidant properties of the films. For this purpose, films (3 mg) were placed in 10 mL water and the samples were agitated. After one hour, the samples were centrifuged, and the supernatant was analyzed by UV spectroscopy after adjusting the NaOH concentration to 0.035 M.

RESULTS AND DISCUSSION

In-situ growth of lignin nanoparticles. CNF and ChNF were used as nucleating support for the formation of lignin nanoparticles (LPs) by solvent shifting. We enriched the water, used as antisolvent medium for the exchange process, with CNF and ChNF to which we poured an acetone solution of lignin. When the acetone fraction in the mixture reached values < 20%, the colloidal particles were formed due to the limited lignin solubility in water.[23] Remarkably, using an antisolvent with the presence of nanofibers, the morphology of the LNPs differ greatly form that observed in their absence (**Figure 2**). Images from Transmission Electron Microscopy (TEM) of CNF and ChNF, before and after LP formation, are shown in **Figures 2a-b** and **2d-e**, respectively, along with the nanoparticle size distribution. For comparison, the morphology and size distribution (TEM and DLS) of lignin particles produced in the nanofiber-free antisolvent are displayed in **Figures 2g-h**.

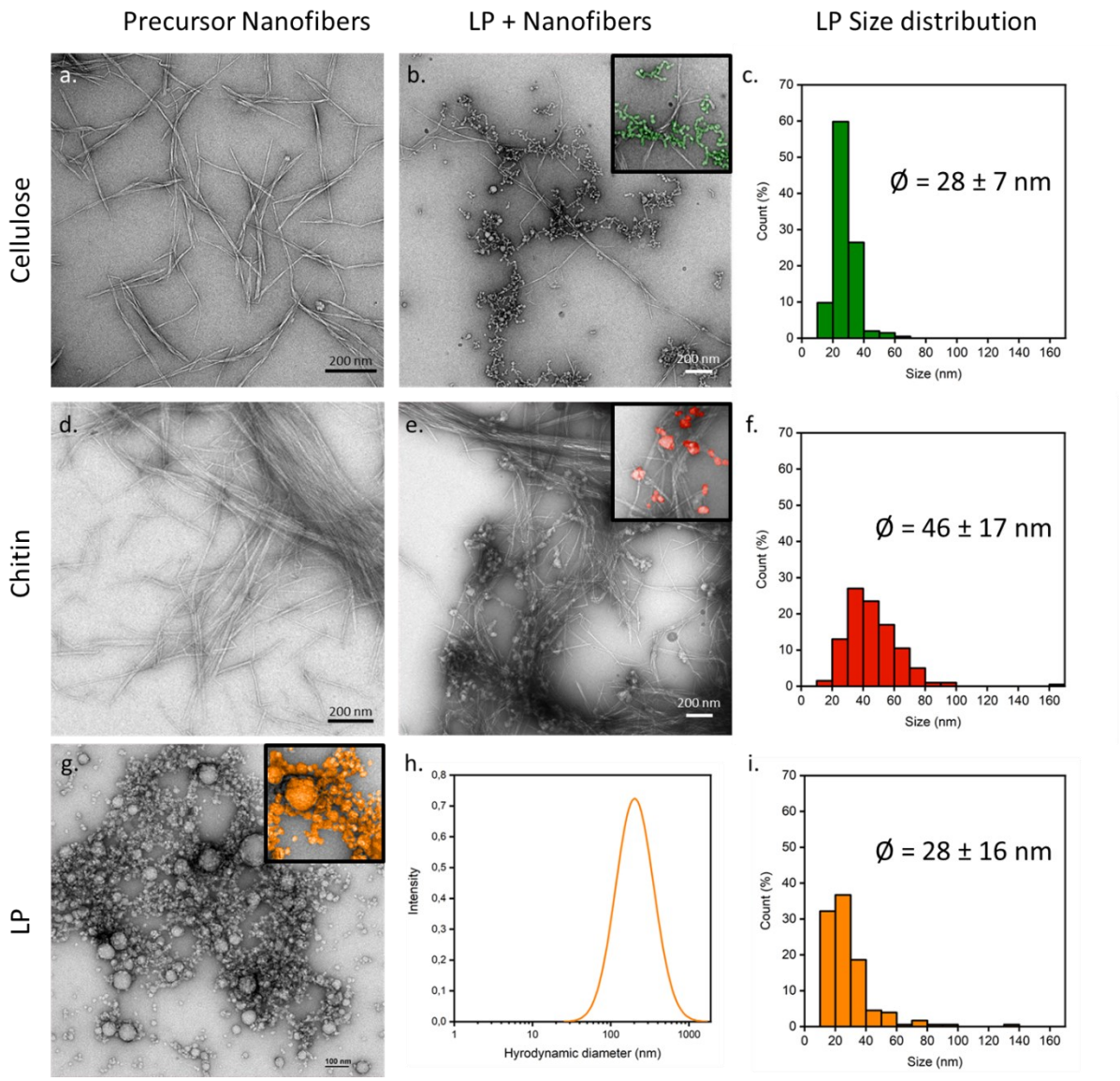

Figure 2. TEM images of nanofibers (CNF, **a** and ChNF, **d**) and the respective system after formation of lignin particles (9%), LP_{CNF} (**b**) and LP_{ChNF} (**e**). The particle size distribution measured from TEM images is also included (LP_{CNF}, **c** and LP_{ChNF}**, f**) as well as lignin particles prepared in the absence of fibers (TEM, **g**) with their size distribution reported from DLS (**h**) and from TEM imaging (**i**).

The average diameter of lignin nanoparticles (LP) prepared in the presence of cellulose nanofibers (LP_{CNF}) had a lateral dimension equivalent to 28 ± 7 nm, with a relatively narrow size distribution (over 95 % of the LP_{CNF} were between 10 and 40 nm). This average size is similar to the values observed for LPs obtained in the absence nanofibers (28 ± 16 nm). These

values are fairly similar to those reported in the literature from similar process and conditions.[28] With the solvent exchange method, in the presence or absence of CNF, the LP were well defined and presented a spherical shaped. In both cases, single lignin particles were observed, but most of them were clustered. Such aggregation is likely the result of drying during sample preparation. The LP_{CNF} particles seemed not to interact with the nanofibers, pointing to the possibility that the cellulosic surface was non-interactive. Cellulose induced a narrow LP size distribution. Such phenomenon can be explained by a spatial restriction, where the fiber network kept the particles apart from each other and prevented coalescence during formation. Electrostatic repulsion between the negatively charged LPs (-52 ± 2 mV zeta potential) and the cellulose nanofibers (-17.0 ± 0.6 mV zeta potential) greatly improved the colloidal stability of the resulting system. In the absence of CNF, LPs displayed a greater tendency to aggregate, as shown by their average hydrodynamic diameter (187 ± 5 nm from DLS, **Figure 2h**). Discrepancies in diameter accessed from DLS and TEM are likely a result of LP swelling.[29]

The lignin particles (LP_{ChNF}) produced in the presence of chitin nanofibers were observed to be attached to the nanofibers and their shape was less spherical compared to LP_{CNF}. The size and distribution, on average, was slightly larger, 46 ± 17 nm (**Figure 2f**). Despite the similar morphology of CNF and ChNF, the observed differences in particle morphology is explained by the distinctive surface chemistry of such substrates. While CNF and ChNF are polysaccharide-based nanoparticles, chitin differs from cellulose by the substitution of one hydroxyl group by an acetyl amine group in the C2 position. When partially deacetylated, even to a small degree, the acetyl amine group in ChNF becomes a primary amine that can be protonated in mild acidic pH, yielding positively charged nanofibers. The latter, with a zeta potential of 27 ± 1 mV, interacts strongly with the deprotonated lignin molecules, leading to an instantaneous lignin adsorption, *via* electrostatic interactions. Thus, ChNF acts as a nuclei for subsequent growth of lignin molecules. Here, we prepared the particles at pH 4 to induce

protonation of the ChNF and, at the same time, keep their colloidal stability. The zeta potential of lignin particles at such pH was measured to be -37.5 ± 0.6 mV. Hence, the observed reduction in zeta-potential, compared to that at neutral pH, relates to the effect of charge neutralization, which leads to destabilization of the system. Therefore, precipitation of lignin on the ChNF is promoted. By increasing the interfacial interactions between lignin and the nanofibers, it is possible to endow a more uniform particle distribution within the nanofiber network, resulting in a more homogenous colloidal suspension. The ChNF charge prevailed in the suspension after LP_{ChNF} preparation at pH 4, resulting in an overall net charge of 24 ± 2 mV. Although the zeta potential remained positive, the absolute value was lower than that of the precursor ChNF, indicating that the lignin particles adsorbed on the surface. The presence of free positive charges is promising as far as the possibility of further increasing the lignin nanoparticle loading.

Based on our data, and the supporting literature, we speculate on the mechanism behind LP formation and their associated morphology, highly depending on the nature of the template. Lignin particle formation *via* controlled precipitation in an anti-solvent is a near instantaneous process that goes through a metastable stage.[30] When templated, the formation of anchored or free lignin nanoparticles occurs before a metastable stage. In the earliest stage of particle formation, adsorption occurs, depending on the nature of the surface. This step is analogous to the formation of templated metallic nanoparticles;[15,31] however, in the case of LPs there is no reduction step and growth solely occurs by the coalescence (cumulative adsorption) of non-soluble molecules, as the solvent fraction (acetone) decreases. Since the precipitation of lignin molecules is rapid, due to their limited water solubility, a very strong interfacial interaction is required for adsorption, before precipitation. This is achieved by using a template that favors electrostatic attraction with lignin, such as ChNF. H-bonding between lignin and CNF is not sufficient to promote adsorption before the onset of particle growth.

We studied the formation of LPs on chitin nanofibers from a homogeneous suspension *via* a one-step process that was influenced by mixing. The nucleation of lignin particles directly on the nanofibers allowed a homogeneous distribution of the LPs with sizes below 100 nm. A relevant observation is that of Ashok et al. who indicated the possibility of producing lignin particles at an industrial scale by solvent shifting,[22] which translates into a promise for our LP_{ChNF}. The process still needs to be further studied in relation of optimized processing conditions, such as the lignin addition rate and lower limits of initial lignin concentration, which have been shown to reduce the particles size.[28] In addition, considering our system, parameters such as nanofibers concentration i.e. the viscosity of the antisolvent system, lignin-to-nanofibers ratio or nanofibers charge content could influence the lignin particles size. By increasing the degree of deacetylation of the chitin nanofibers, it is possible to further increase the lignin content without flocculation, given the effects of charge hindrance. This might also increase the number of nucleation sites and hence decrease the particles size. The size of the nanoparticles is also important for further functionalization and composite formation. In fact, smaller sizes tend to increase the compatibility of reinforcing elements. For example, Nair et al. demonstrated that smaller and more homogeneous lignin particle size facilitated their dispersion in polyvinyl alcohol.[32] The final properties, such as anti-oxidant activity, were found to be influenced by the particles size, as the activity increased with the surface area available for reaction.[33] Here we devised the initial concentration needed to achieve small particles while maintaining a reasonable final volume. In the presence of the nanofibers, we obtained LPs with sizes < 50 nm, smaller compared to those obtained in the absence of solid interfaces.[28,34] Hence, formation of LPs in the presence of CNF and ChNF, opens a unique opportunity for the efficient integration of the particles in matrices, for example, for material development.

Interfacial interactions between lignin and the nanofibers. We investigated the interfacial interactions between lignin particles and the templating nanofibers, for instance, by promoting destabilization and segregation under centrifugal fields (10 000 rpm, 5 min). The formed lignin particles presented colloidal sizes that warrant better stability compared to mechanically fibrillated nanofibers, with lengths in the micrometer range. Upon centrifugation, the brownish color of lignin, which contrasts with that of CNF and ChNF, can be easily identified for visual observation, e.g., to conclude whether the particles are sedimented with the nanofibers or remained suspended, in the supernatant (**Figure S1a-b.**). Photos of the supernatants and sediments of systems subjected to centrifugation are shown in **Figure S1a-b**. In the LP_{CNF} system, a brown supernatant was observed, indicating the presence of lignin particles. In contrast, a whitish sediment indicated nearly pure CNF fully separated from the lignin particles. In the case of LP_{ChNF}, the sediment containing the ChNF was brown and the supernatant was colorless, indicating that the LPs interacted strongly with ChNF. It was possible to quantify the lignin present in the sediment (UV-Vis analysis) after dissolving the lignin particles in NaOH[26] (see **Figure S1c** and calibration curve in **Figure S2**). A lignin content of 4.5 ± 0.3 % was measured in the sediment containing CNF, while the ChNF sediment contained 67.4 ± 0.6 % of the total lignin, a result of the precipitated lignin together with the positively charged chitin nanofibers. Lignin particles above the colloidal size or aggregated could sediment along with the nanofibers, which could explain the presence of lignin with the sedimented cellulose nanofibers. The lignin present on the sediment of chitin nanofibers imply that electrostatic interactions are strong enough to favor adsorption of LP (mainly < 100 nm and thus colloidally stable). This supports our hypothesis derived from TEM imaging, which indicated that lignin has better affinity with chitin than with cellulose.

To gain deeper insights on the interactions between lignin and the nanofibers, we used thin layer chromatography (TLC) in our system, e.g., to confirm a greater affinity of lignin with

chitin compared to cellulosic surface (**Figure 3c**). Here chromatographic paper was coated with the respective nanofiber suspension to produce CNF and ChNF surfaces that were later used as TLC stationary phases. The mobile phase (eluent) was a mixture of acetone:water (4:6), which was used to investigate solvent-surface-molecule competitive interactions. **Figure 3b**, includes blue profiles of the images (acquired by image analysis software), taken after elution and under UV light to increase the contrast (**Figure 3a**). On CNF-coated paper, lignin interacted poorly with CNF and moved far in the stationary phase with the eluent, mostly accumulating at the top of the TLC paper. For ChNF, we observed milder shades of blue along the elution direction, confirming that the lignin molecules spread along the TLC paper, a result from strong interactions with the stationary phase. Lignin molecules also spread on the CNF-coated paper; however, within a narrower region, showing that lignin also interacted partly with cellulose. Such interactions are driven by weak, secondary interactions such as H-bonding; in contrast, stronger electrostatic interactions take place at the ChNF-lignin interface. Hydrophobic interactions between acetyl groups of chitin and aromatic moieties in lignin may also improve the affinity between the two components; however they might be difficult to resolve due to overlapping by ionic pairing. With this, we demonstrated that the surface chemistry of the nanofibers is a key for the formation of LP in-situ. In consequence, additionally to the nature of the nanofibers, further chemical modification in the nanofibers would also influence their interfacial interactions with lignin. Thus the method used for nanofibers preparation is of importance on the behavior of the system.

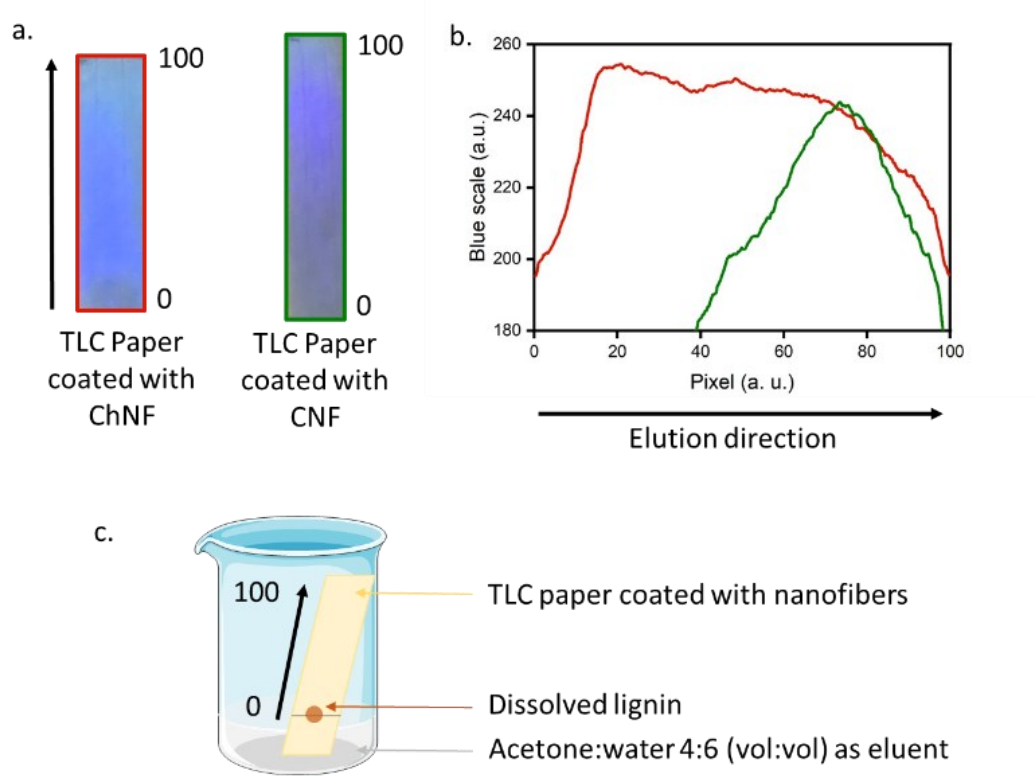

Figure 3. Thin layer chromatography (TLC) using paper coated with CNF and ChNF and acetone:water as eluent: **a.** images taken under UV light for image analysis. **b.** average blue intensity value of each pixel lines normalized to 100 (0 represents the start line and 100 the solvent front). **c.** Scheme of the paper chromatography experimental set up.

We demonstrate that the electrostatic interactions between chitin and lignin can be harnessed to develop hybrid colloids enriched with strongly coupled nanoparticles. We investigated the effect of lignin content on particle formation by varying the amount of suspended lignin, from 9% to 15% and 23%. A high lignin concentration enhanced the properties of the obtained material, such as lignin's antioxidant activity. However, a compromise between functionality and stability of the network needs to be maintained. When forming the LP_{ChNF} from more concentrated lignin solutions (accounting for 15 and 23 wt%.), the sizes (TEM) of the lignin particles attached on the nanofibers were 59 ± 19 nm and 61 ± 25 nm for 15% and 23% of lignin, respectively (**Figure S3**). We observed that with an increased lignin content, the

particles size increased (as well as the size distribution). This is a result of the reduced ratio between nucleation sites on the chitin nanofibers and the amount of lignin available for adsorption. The morphology of the network may be further tailored by controlling the addition rate during solvent exchange, since a faster addition is expected to increase the density of nucleation sites and therefore homogenize the size distribution.

Preparation of films from nanofibers carrying LPs. We discuss the effect of incorporation of lignin particles, from *in-situ* formation on CNF and ChNF, for films preparation. We evaluated the properties of the films considering their application for food packaging. The impact of the particles on films structuring and mechanical strength was studied (**Figure 4**) followed by the UV-shielding and antioxidant activity (**Figure 5**).

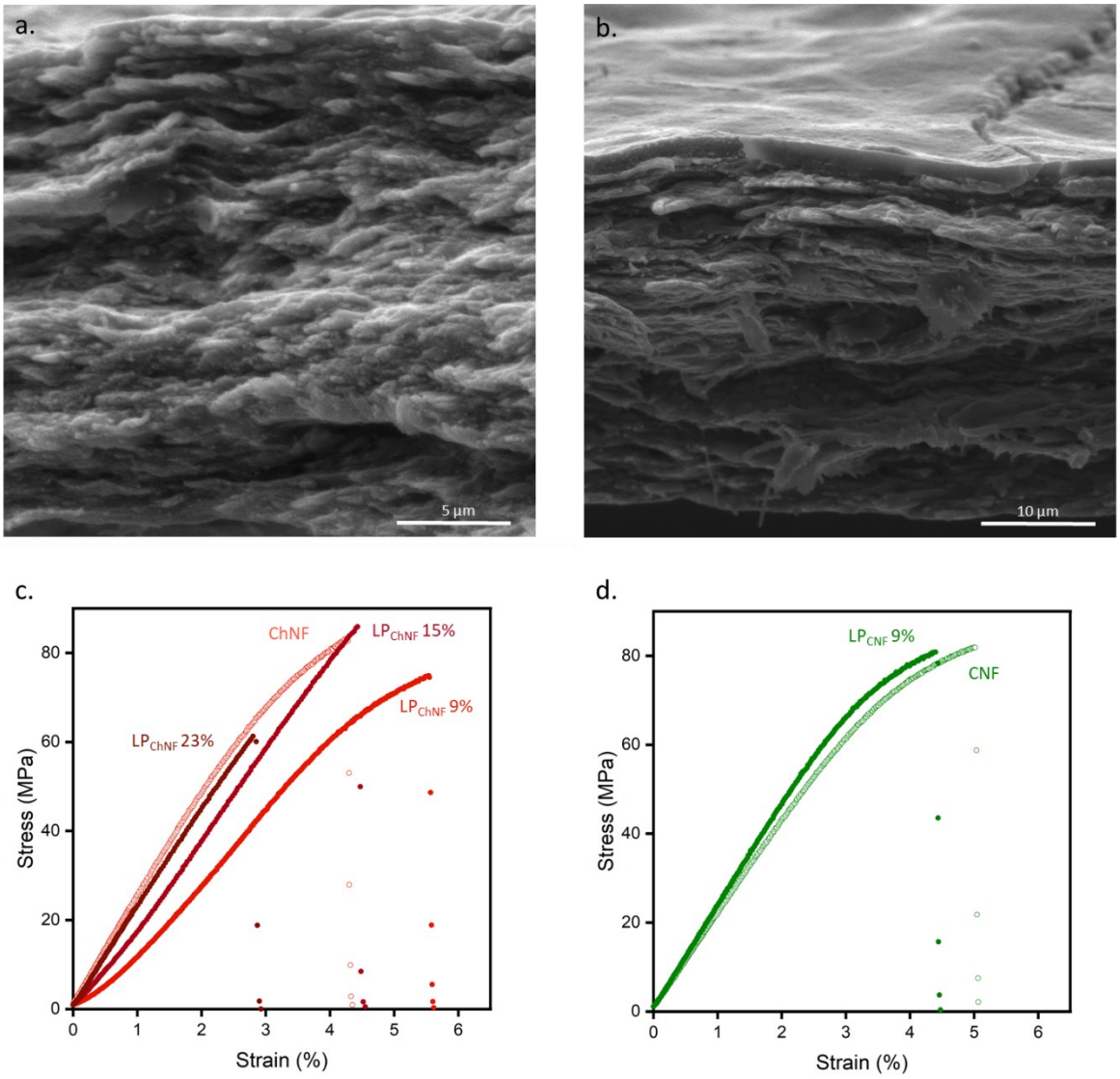

Figure 4. Cross-section images (SEM) of the films: **a.** chitin and **b.** cellulose nanofibers containing 9% LP. Tensile stress versus strain profiles used to evaluate the mechanical strength of films made with **c.** chitin nanofibers with 0% (o), 9% (●), 15% (●) and 23% (●) LP and **d.** cellulose nanofibers with 0% (o) and 9% (●) LP, as indicated.

The CNF and ChNF films loaded with different LP content were produced by solvent casting on PTFE Petri dishes. **Figure 4a-b** shows SEM cross-section images of the films containing 9% LP_{CNF} and LP_{ChNF}. In both cases, it is possible to identify a fibrillar network as well as the formation of a lamellar structures. The observations indicate that the incorporation of 9% LP did not interfere with film structuring. The reduced nanoparticles size was key to avoid the disruption of a strong fibrillar network. In the LP_{ChNF} film, the structure was homogeneous,

and the LPs were shown to be incorporated homogeneously; however, the structure of LP_{CNF} film displayed two distinct components: a fibrillar web and an upper, lignin particle layer. AFM analysis of the surface of the LP_{CNF} film clearly suggested the presence of a dense LP layer on the surface, not observed in the LP_{ChNF} film (**Figure S4**). In the case of CNF, the fibrils sedimented and the LPs, which are colloidally stable, remained suspended during water evaporation. This led to the accumulation of LPs on the surface of the formed film. In fact, the lack of interfacial interaction between LP and CNFs led to segregation, driven by capillary pulling forces that developed during drying. The observations agree with results from separation, *via* centrifugation, that showed sedimentation of CNF with simultaneous accumulation of LPs particles in the suspended medium. Filtration is suggested as a method to obtain a better mixing between LPs and CNF, provided that particle drainage is avoided through the forming mesh.

In the case of LP_{CNF} films, the mechanical properties were similar to those of neat CNF films, which is explained by the fact that LPs accumulated on the surface of LP_{CNF} films. This hinders the contribution of the particles with respect to fibrillar entanglement, which is a main factor explaining the development of film cohesion. The lignin content in LP_{ChNF} films, did not interfere the mechanical performance, up to 15% of LP loading. However, at 23% LP the stress-strain profiles followed a similar trend, but the rupture occurred at lower stresses and strains (ca. 3%) indicating a reduction in toughness. The stiffness of LP_{ChNF} films increased with LP content, from 9 to 23%; this could be explained by the loss of interfibrillar hydrogen bonding due to the presence of LPs that disturb the film structure, leading to brittle films.[20]

A low film wettability is desirable for packaging applications. To investigate such feature, we measured the contact angle of films with and without LPs (**Table 1**). In general, the contact angle of the films, regardless their nature, increased with LP loading. For the neat CNF film, the decrease in drop volume was relatively high (> 40%), meaning that high water absorption

took place by the effect of the bulk film; however, in the presence of 9% LP the decrease in volume was limited to ca. 6%. This is explained by the presence of a dense LP layer on top of the film which reduced the absorption of water, also leading to a higher contact angle. For LP_{ChNF} films, water absorption also decreased with increasing LP content, which relates to LP filling of the pores.[21] Therefore, the contact angle follows the same trend. Water is a major challenge when considering polysaccharide building blocks for material development; therefore, our results for water-biocolloid interactions can open new opportunities.

Table 1. Contact angles and final water drop volume measured after 2 min in contact with the films

LP %	**LP_{ChNF}**		**LP_{CNF}**	
	Contact Angle	*Final Drop Volume (% of initial volume)*	*Contact Angle*	*Final Drop Volume (% of initial volume)*
0	32 ± 6°	87 ± 11	22 ± 8°	62 ± 16
9	56 ± 2°	90 ± 5	55 ± 5°	94 ± 4
15	72 ± 5°	91 ± 1	-	-
23	63 ± 1°	94 ± 4	-	-

So far, we have shown that LP coupling with cellulose and chitin nanofibers does not deteriorate the mechanical performance of the respective films while increasing their water resistance. Moreover, the addition of lignin is expected to endow the films with photocatalytic activities. The polyphenolic lignin promotes UV absorption and free radical scavenging, thus making it a suitable component for food packaging. Additionally, the nanosized particles enhance the respective efficiency and, at the same time, their association with a network of chitin nanofibers prevents leakage.

The transmittance data for LP_{ChNF} films measured by UV-Vis spectroscopy are shown in **Figure 5a** for 0 to 23 % LP loading. All the lignin-containing films presented negligible transmittance below 400 nm, e.g., full UV shielding was achieved. A higher transparency in the visible range was observed for smaller fibers and particles.[35] The antioxidant activity of the

films was measured using the ABTS radical in water, to avoid dissolution of lignin in the commonly used solvents applied in the DPPH test – ethanol or methanol. After bringing the films in contact with the radical solution, the decrease in radical activity was measured by UV-Vis spectrometry, showing a remarkable reduction in radical activity. To draw film comparisons, the radical scavenging activity was calculated after 1 h contact and compared with a control based on tannic acid, which is a well-known natural antioxidant (high radical scavenging activity[36]). In **Figure 5b**, the tannic acid equivalent (TAE) for LP_{ChNF} films is shown as a function of LP content: an increased antioxidant activity was noticed with increased LP content. Films with smaller sizes but same LP content showed an enhanced antioxidant activity compared, for instance, with recent results.[20] In agreement with our observations, Zhang et al. showed that decreasing particles size led to an increased antioxidant activity, which was explained by a higher accessibility of phenolic groups.[33] Release experiments were performed, for systems under same conditions: < 5 % lignin release (based on the total loading in each film) was measured, indicating that the radical scavenging activity is ascribed to the surface of the film .

By considering films with different lignin loading, 15 % LP was found to be a suitable balance between mechanical strength, wettability and antioxidant activity. However, depending on the desired application for such LP_{ChNF} films, the lignin content can be further optimized. Whereas films with < 9% LP are likely to be effective for complete UV-shielding, higher antioxidant activity is obtained with higher lignin content. Complete UV shielding and high antioxidant activity are beneficial effects in food packaging applications. In fact, UV light penetration through the packaging material creates free radicals, increasing food degradation rate and reducing shell life.[18] The incorporation of LPs in chitin nanofiber networks and respective electrostatic interactions are expected to prevent particle leakage, which is key with regards to food safety. As the interactions between lignin and chitin prevent any LP leakage, this system

could also be of interest for drug release applications. In fact, it has been demonstrated that dissolved drugs could be encapsulated in LP during solvent shifting preparation[29] therefore the in-situ preparation of LP on nanofibers could be a one step process for drug encapsulation and LP anchoring on a matrix. Our system could also be of interest in applications such as sunscreen[37] where the UV blocking ability of LP combined with the nanofibers rheological properties could be exploited. Active membranes for filtration could be another potential application as nanofibers have the ability to form 3D network that could be functionalized with LP[11], the interactions between LP and the matrix would prevent any particles leakage.

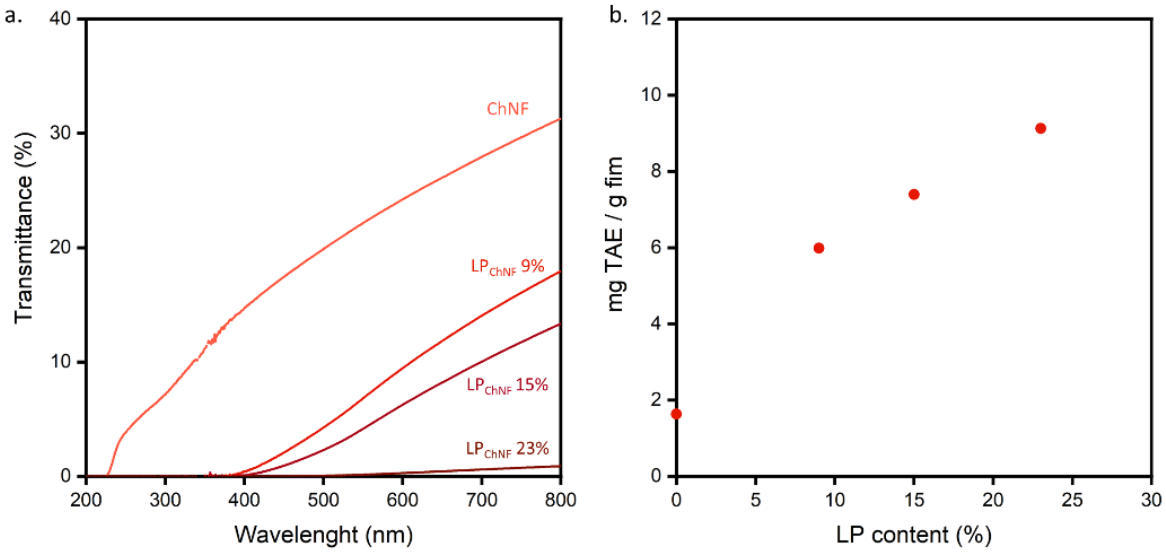

Figure 5. Functional properties of LP_{ChNF} films: **a.** UV-Visible transmittance of the LP_{ChNF} films containing given fractions of LP. **b.** Antioxidant activity of films measured by the tannic acid equivalent (TAE) as function of LP loading in ChNF films.

CONCLUSION

We developed a new process to produce lignin nanoparticles in the presence of bio-based nanofibers *via* solvent shifting. Lignin nanoparticles of sizes < 100 nm were synthesized in the presence of cellulose and chitin nanofibers. The positive charges in chitin enabled electrostatic interactions with lignin, leading to a strong and homogeneous distribution of LP on the chitin nanofiber network. Suspensions with high lignin content were successfully prepared leading to

increased LP sizes. Investigation of relevant parameters such as lignin type, fibers size and concentration as well as morphology should be considered to optimize the process and properties of the hybrid nanofibers.

LPs with a narrow size distribution were formed in the presence of cellulose nanofibers, but displayed electrostatic repulsion, which resulted in phase separation during film formation and non-homogeneous repartition of LPs in the film. In contrasts, the films prepared with chitin nanofibers showed well-dispersed LPs, which resulted in a high film mechanical strength, similar to that of the neat nanofiber film. Complete UV shielding was achieved for all the films containing LPs, with an antioxidant activity that tracked LP loading. The results offer great promise in applications such as food packaging.

SUPPORTING INFORMATION

The SI file contains 3 pages with 4 figures. Photos of LP_{CNF} and LP_{ChNF} after centrifugation with associated UV spectra, UV-Vis calibration curve of dissolved lignin, TEM images and associated LP size distribution of ChNF containing 15% and 23% LP, AFM images of LP_{ChNF} and LP_{CNF} films.

AUTHOR INFORMATION

Corresponding Author

Orlando J. Rojas: Orlando.rojas@ubc.ca

Present Address

± Nestle Research Center, 1000 Lausanne, Switzerland

ACKNOWLEDGEMENTS

LGP2 is part of the LabEx Tec 21 (Investissements d'Avenir - grant agreement n°ANR-11-LABX-0030) and of PolyNat Carnot Institute (Investissements d'Avenir - grant agreement n° ANR-16-CARN-0025-01). This work was supported by Grenoble INP, "Bourse Présidence" and the European Research Council under the European Union's Horizon 2020 research and innovation program (ERC Advanced Grant Agreement No. 788489, "BioElCell"). O.J.R. also acknowledges the Canada Excellence Research Chair initiative, and the Canada Foundation for Innovation (CFI).

REFERENCES

(1) Zhu, J.; Yang, M.; Emre, A.; Bahng, J. H.; Xu, L.; Yeom, J.; Yeom, B.; Kim, Y.; Johnson, K.; Green, P.; Kotov, N. A. Branched Aramid Nanofibers. *Angew. Chem. Int. Ed.* **2017**, *56* (39), 11744–11748. https://doi.org/10.1002/anie.201703766.

(2) Mittal, N.; Ansari, F.; Gowda.V, K.; Brouzet, C.; Chen, P.; Larsson, P. T.; Roth, S. V.; Lundell, F.; Wågberg, L.; Kotov, N. A.; Söderberg, L. D. Multiscale Control of Nanocellulose Assembly: Transferring Remarkable Nanoscale Fibril Mechanics to Macroscale Fibers. *ACS Nano* **2018**, *12* (7), 6378–6388. https://doi.org/10.1021/acsnano.8b01084.

(3) Ling, S.; Kaplan, D. L.; Buehler, M. J. Nanofibrils in Nature and Materials Engineering. *Nat. Rev. Mater.* **2018**, *3* (4), 1–15. https://doi.org/10.1038/natrevmats.2018.16.

(4) Ifuku, S.; Saimoto, H. Chitin Nanofibers: Preparations, Modifications, and Applications. *Nanoscale* **2012**, *4* (11), 3308–3318. https://doi.org/10.1039/C2NR30383C.

(5) Kontturi, E.; Laaksonen, P.; Linder, M. B.; Nonappa; Gröschel, A. H.; Rojas, O. J.; Ikkala, O. Advanced Materials through Assembly of Nanocelluloses. *Adv. Mater.* **2018**, *30* (24), 1703779. https://doi.org/10.1002/adma.201703779.

(6) Zhu, H.; Zhu, S.; Jia, Z.; Parvinian, S.; Li, Y.; Vaaland, O.; Hu, L.; Li, T. Anomalous Scaling Law of Strength and Toughness of Cellulose Nanopaper. *Proc. Natl. Acad. Sci.* **2015**, *112* (29), 8971–8976. https://doi.org/10.1073/pnas.1502870112.

(7) Reverdy, C.; Belgacem, N.; Moghaddam, M. S.; Sundin, M.; Swerin, A.; Bras, J. One-Step Superhydrophobic Coating Using Hydrophobized Cellulose Nanofibrils. *Colloids Surf. Physicochem. Eng. Asp.* **2018**, *544*, 152–158. https://doi.org/10.1016/j.colsurfa.2017.12.059.

(8) Ghanadpour, M.; Carosio, F.; Larsson, P. T.; Wågberg, L. Phosphorylated Cellulose Nanofibrils: A Renewable Nanomaterial for the Preparation of Intrinsically Flame-Retardant Materials. *Biomacromolecules* **2015**, *16* (10), 3399–3410. https://doi.org/10.1021/acs.biomac.5b01117.

(9) Sasso, C.; Zeno, E.; Petit-Conil, M.; Chaussy, D.; Belgacem, M. N.; Tapin-Lingua, S.; Beneventi, D. Highly Conducting Polypyrrole/Cellulose Nanocomposite Films with Enhanced Mechanical Properties. *Macromol. Mater. Eng.* **2010**, *295* (10), 934–941. https://doi.org/10.1002/mame.201000148.

(10) Mattos, B. D.; Tardy, B. L.; Greca, L. G.; Kämäräinen, T.; Xiang, W.; Cusola, O.; Magalhães, W. L. E.; Rojas, O. J. Nanofibrillar Networks Enable Universal Assembly

of Superstructured Particle Constructs. *Sci. Adv.* **2020**, *6* (19), eaaz7328. https://doi.org/10.1126/sciadv.aaz7328.
(11) Cusola, O.; Rojas, O. J.; Roncero, M. B. Lignin Particles for Multifunctional Membranes, Antioxidative Microfiltration, Patterning, and 3D Structuring. *ACS Appl. Mater. Interfaces* **2019**, *11* (48), 45226–45236. https://doi.org/10.1021/acsami.9b16931.
(12) Rol, F.; Belgacem, M. N.; Gandini, A.; Bras, J. Recent Advances in Surface-Modified Cellulose Nanofibrils. *Prog. Polym. Sci.* **2019**, *88*, 241–264. https://doi.org/10.1016/j.progpolymsci.2018.09.002.
(13) Lokanathan, A. R.; Uddin, K. M. A.; Rojas, O. J.; Laine, J. Cellulose Nanocrystal-Mediated Synthesis of Silver Nanoparticles: Role of Sulfate Groups in Nucleation Phenomena. *Biomacromolecules* **2014**, *15* (1), 373–379. https://doi.org/10.1021/bm401613h.
(14) Hoeng, F.; Denneulin, A.; Neuman, C.; Bras, J. Charge Density Modification of Carboxylated Cellulose Nanocrystals for Stable Silver Nanoparticles Suspension Preparation. *J. Nanoparticle Res.* **2015**, *17* (6), 244. https://doi.org/10.1007/s11051-015-3044-z.
(15) Olsson, R. T.; Samir, M. A. S. A.; Salazar-Alvarez, G.; Belova, L.; Ström, V.; Berglund, L. A.; Ikkala, O.; Nogués, J.; Gedde, U. W. Making Flexible Magnetic Aerogels and Stiff Magnetic Nanopaper Using Cellulose Nanofibrils as Templates. *Nat. Nanotechnol.* **2010**, *5* (8), 584–588. https://doi.org/10.1038/nnano.2010.155.
(16) Padalkar, S.; Capadona, J. R.; Rowan, S. J.; Weder, C.; Won, Y.-H.; Stanciu, L. A.; Moon, R. J. Natural Biopolymers: Novel Templates for the Synthesis of Nanostructures. *Langmuir* **2010**, *26* (11), 8497–8502. https://doi.org/10.1021/la904439p.
(17) Errokh, A.; Magnin, A.; Putaux, J.-L.; Boufi, S. Hybrid Nanocellulose Decorated with Silver Nanoparticles as Reinforcing Filler with Antibacterial Properties. *Mater. Sci. Eng. C* **2019**, *105*, 110044. https://doi.org/10.1016/j.msec.2019.110044.
(18) Kwon, S.; Orsuwan, A.; Bumbudsanpharoke, N.; Yoon, C.; Choi, J.; Ko, S. A Short Review of Light Barrier Materials for Food and Beverage Packaging. *KOREAN J. Packag. Sci. Technol.* **2018**, *24* (3), 141–148. https://doi.org/10.20909/kopast.2018.24.3.141.
(19) Wang, B.; Sun, D.; Wang, H.-M.; Yuan, T.-Q.; Sun, R.-C. Green and Facile Preparation of Regular Lignin Nanoparticles with High Yield and Their Natural Broad-Spectrum Sunscreens. *ACS Sustain. Chem. Eng.* **2019**, *7* (2), 2658–2666. https://doi.org/10.1021/acssuschemeng.8b05735.
(20) Farooq, M.; Zou, T.; Riviere, G.; Sipponen, M. H.; Österberg, M. Strong, Ductile, and Waterproof Cellulose Nanofibril Composite Films with Colloidal Lignin Particles. *Biomacromolecules* **2019**, *20* (2), 693–704. https://doi.org/10.1021/acs.biomac.8b01364.
(21) Liu, Y. Strong and Flexible Nanocomposites of Carboxylated Cellulose Nanofibril Dispersed by Industrial Lignin. *ACS Sustain. Chem. Eng.* **2018**, *6* (4), 5524–5532. https://doi.org/10.1021/acssuschemeng.8b00402.
(22) Ashok, R. P. B.; Oinas, P.; Lintinen, K.; Sarwar, G.; Kostiainen, M. A.; Österberg, M. Techno-Economic Assessment for the Large-Scale Production of Colloidal Lignin Particles. *Green Chem.* **2018**, *20* (21), 4911–4919. https://doi.org/10.1039/C8GC02805B.
(23) Leskinen, T.; Smyth, M.; Xiao, Y.; Lintinen, K.; Mattinen, M. L.; Kostiainen, M. A.; Oinas, P.; Österberg, M. Scaling up Production of Colloidal Lignin Particles. *Nord*

Pulp Pap. Res. J. **2017**, *32* (4), 586–596. https://doi.org/10.3183/NPPRJ-2017-32-04-p586-596.
(24) Ifuku, S.; Nogi, M.; Abe, K.; Yoshioka, M.; Morimoto, M.; Saimoto, H.; Yano, H. Preparation of Chitin Nanofibers with a Uniform Width as α-Chitin from Crab Shells. *Biomacromolecules* **2009**, *10* (6), 1584–1588. https://doi.org/10.1021/bm900163d.
(25) Yearla, S. R.; Padmasree, K. Preparation and Characterisation of Lignin Nanoparticles: Evaluation of Their Potential as Antioxidants and UV Protectants. *J. Exp. Nanosci.* **2016**, *11* (4), 289–302. https://doi.org/10.1080/17458080.2015.1055842.
(26) Lee, R. A.; Bédard, C.; Berberi, V.; Beauchet, R.; Lavoie, J.-M. UV–Vis as Quantification Tool for Solubilized Lignin Following a Single-Shot Steam Process. *Bioresour. Technol.* **2013**, *144*, 658–663. https://doi.org/10.1016/j.biortech.2013.06.045.
(27) Re, R.; Pellegrini, N.; Proteggente, A.; Pannala, A.; Yang, M.; Rice-Evans, C. Antioxidant Activity Applying an Improved ABTS Radical Cation Decolorization Assay. *Free Radic. Biol. Med.* **1999**, *26* (9), 1231–1237. https://doi.org/10.1016/S0891-5849(98)00315-3.
(28) Richter, A. P.; Bharti, B.; Armstrong, H. B.; Brown, J. S.; Plemmons, D.; Paunov, V. N.; Stoyanov, S. D.; Velev, O. D. Synthesis and Characterization of Biodegradable Lignin Nanoparticles with Tunable Surface Properties. *Langmuir* **2016**, *32* (25), 6468–6477. https://doi.org/10.1021/acs.langmuir.6b01088.
(29) Sipponen, M. H.; Lange, H.; Ago, M.; Crestini, C. Understanding Lignin Aggregation Processes. A Case Study: Budesonide Entrapment and Stimuli Controlled Release from Lignin Nanoparticles. *ACS Sustain. Chem. Eng.* **2018**, *6* (7), 9342–9351. https://doi.org/10.1021/acssuschemeng.8b01652.
(30) Österberg, M.; Sipponen, M. H.; Mattos, B. D.; Rojas, O. J. Spherical Lignin Particles: A Review on Their Sustainability and Applications. *Green Chem.* **2020**, *22* (9), 2712–2733. https://doi.org/10.1039/D0GC00096E.
(31) Valencia, L.; Kumar, S.; Nomena, E. M.; Salazar-Alvarez, G.; Mathew, A. P. In-Situ Growth of Metal Oxide Nanoparticles on Cellulose Nanofibrils for Dye Removal and Antimicrobial Applications. *ACS Appl. Nano Mater.* **2020**, *3* (7), 7172–7181. https://doi.org/10.1021/acsanm.0c01511.
(32) Nair, S. S.; Sharma, S.; Pu, Y.; Sun, Q.; Pan, S.; Zhu, J. Y.; Deng, Y.; Ragauskas, A. J. High Shear Homogenization of Lignin to Nanolignin and Thermal Stability of Nanolignin-Polyvinyl Alcohol Blends. *ChemSusChem* **2014**, *7* (12), 3513–3520. https://doi.org/10.1002/cssc.201402314.
(33) Zhang, X.; Yang, M.; Yuan, Q.; Cheng, G. Controlled Preparation of Corncob Lignin Nanoparticles and Their Size-Dependent Antioxidant Properties: Toward High Value Utilization of Lignin. *ACS Sustain. Chem. Eng.* **2019**, *7* (20), 17166–17174. https://doi.org/10.1021/acssuschemeng.9b03535.
(34) Qian, Y.; Zhong, X.; Li, Y.; Qiu, X. Fabrication of Uniform Lignin Colloidal Spheres for Developing Natural Broad-Spectrum Sunscreens with High Sun Protection Factor. *Ind. Crops Prod.* **2017**, *101*, 54–60. https://doi.org/10.1016/j.indcrop.2017.03.001.
(35) Chinga-Carrasco, G. Optical Methods for the Quantification of the Fibrillation Degree of Bleached MFC Materials. *Micron* **2013**, *48*, 42–48. https://doi.org/10.1016/j.micron.2013.02.005.
(36) Vilchez, A.; Acevedo, F.; Cea, M.; Seeger, M.; Navia, R. Applications of Electrospun Nanofibers with Antioxidant Properties: A Review. *Nanomaterials* **2020**, *10* (1), 175. https://doi.org/10.3390/nano10010175.

(37) Qian, Y.; Qiu, X.; Zhu, S. Lignin: A Nature-Inspired Sun Blocker for Broad-Spectrum Sunscreens. *Green Chem.* **2014**, *17* (1), 320–324. https://doi.org/10.1039/C4GC01333F.

Table of Content

Lignin nanoparticle nucleation and growth on cellulose and chitin nanofibers

Eva Pasquier[a,b], Bruno D. Mattos[b], Naceur Belgacem[a,c], Julien Bras[a,c,±], Orlando J. Rojas[b,d]

[a] *Université Grenoble Alpes, CNRS, Grenoble INP (*Institute of Engineering *), LGP2, F-38000 Grenoble, France*
[b] *Department of Bioproducts and Biosystems, School of Chemical Engineering, Aalto University, P.O. Box 16300, Aalto, Espoo FIN-00076, Finland*
[c] *Institut Universitaire de France (IUF), 75000 Paris, France*
[d] *Bioproducts Institute, Departments of Chemical and Biological Engineering, Chemistry and Wood Science, University of British Columbia, 2360 East Mall, Vancouver, BC V6T 1Z3, Canada*